フィン付き流路内の流動・熱伝達特性に関する研究

6

The Effects of Duct Height on Heat Transfer Enhancement and Flow Characteristics of Finned Surface.

6.1 Introduction

In this chapter we have discussed the effects of duct height on heat transfer enhancement and flow characteristics of finned surfaces of co-angular and co-rotating pattern as we have already got the co-rotating pattern shows the highest thermal performance among four different fin patterns. In this investigation duct height was varied from 20 – 50 mm and the pitch ratio (*PR)* in streamwise direction, fin height and inclination angle were fixed as 2, 10 mm and 20 degree respectively

6.2. Detailed heat transfer

The effect of duct height on heat transfer coefficient profile and iso heat transfer coefficient contour in case of co-angular pattern is observed which is shown in Fig. 6.1. We can compare the heat transfer coefficient profile from Fig. 6.1(a), (b), (c), (d), (e),(f) and (g) as the range of heat transfer heat transfer coefficients were maintained same for all the figures. Though the shape of heat transfer profile among the fin rows on the endwall are found almost same regardless of duct height but the areas of higher heat transfer and lower heat transfer are clearly visible different on the endwall. In Fig.6.1 it is observed that higher heat transfer region decreases with increasing duct height. It is also noticed that the higher heat transfer regions adjacent to the fin base also decreases with increasing duct height. Iso heat transfer coefficient contour also shows the enlarged area of higher heat transfer on the endwall incase of lower duct height while the lower heat transfer regions are apparently shown enlarges with increasing duct height. This is because duct height influences the flow field as a result heat transfer

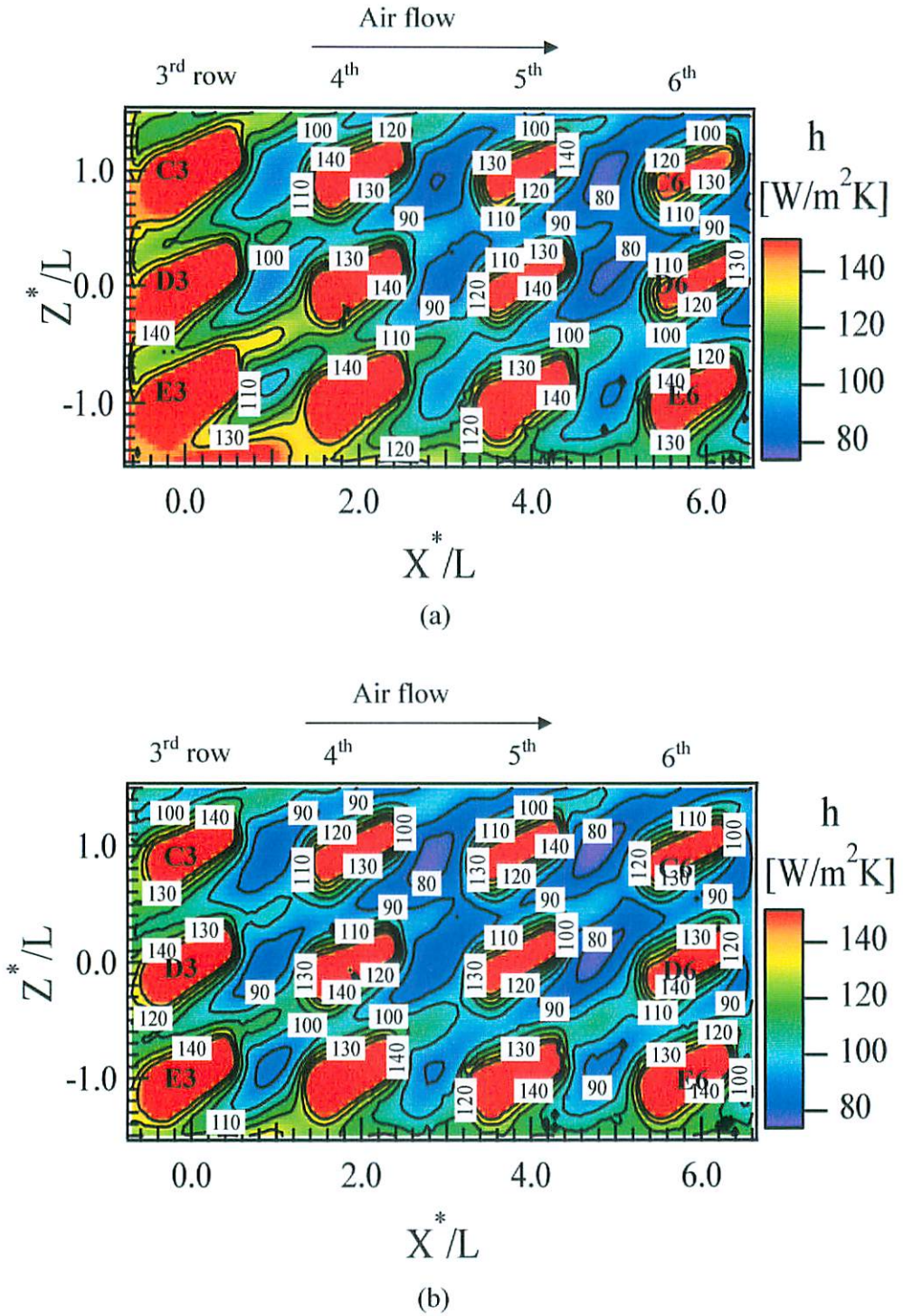

Fig. 6.1 Detailed heat transfer coefficient profile with iso heat transfer coefficient contour of the representative fin region with co-angular pattern for U = 10 m/s, H_f = 10 mm, PR = 2 and for duct height (H_d) of (a) 20 mm, (b) 25 mm, (c) 30 mm, (d) 35 mm, (e) 40 mm, (f) 45 mm and (g) 50 mm.

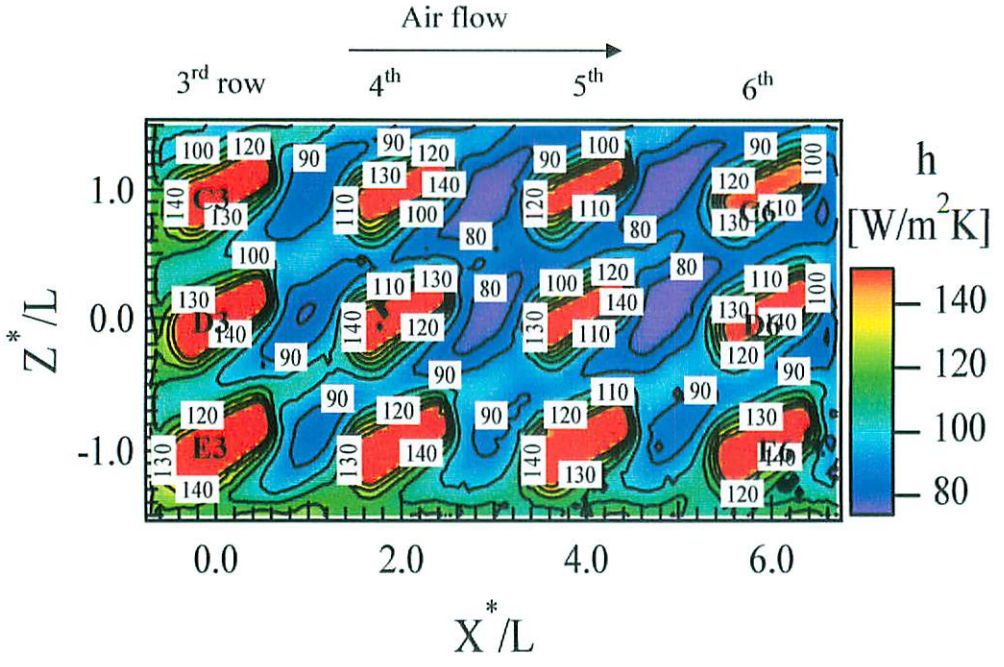

(c)

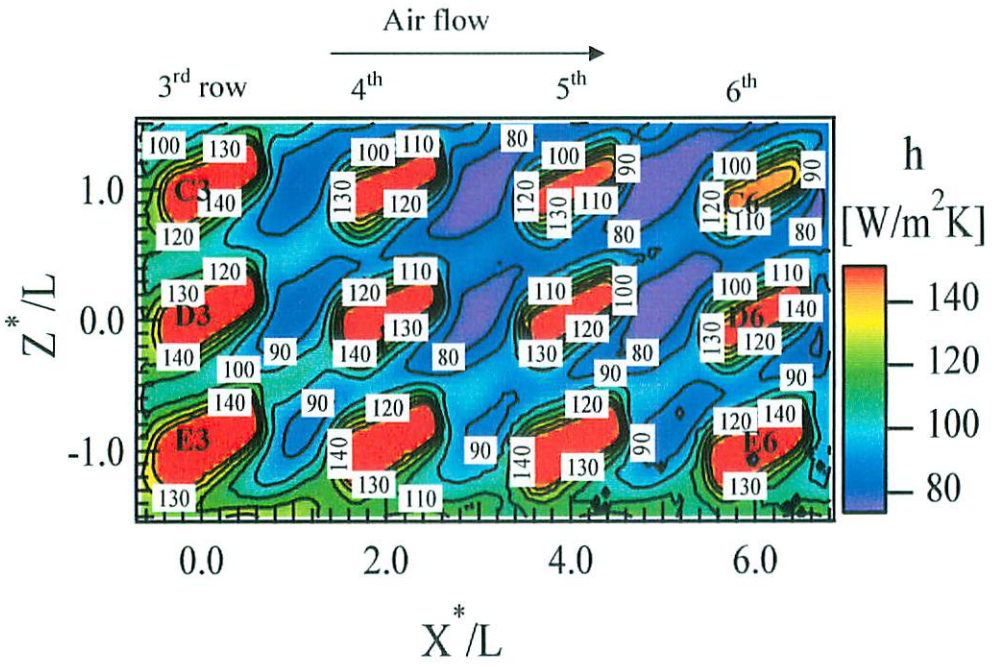

(d)

Fig. 6.1 Detailed heat transfer coefficient profile with iso heat transfer coefficient contour of the representative fin region with co-angular pattern for U= 10 m/s, H_f = 10 mm, PR = 2 and for duct height (H_d) of (a) 20 mm, (b) 25 mm, (c) 30 mm, (d) 35 mm, (e) 40 mm, (f) 45 mm and (g) 50 mm.

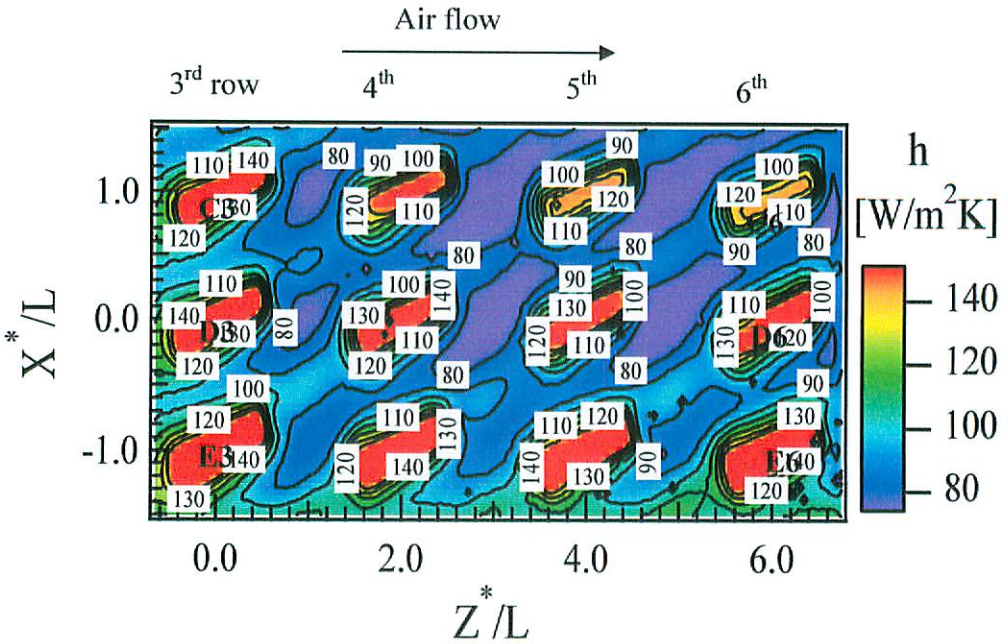

(e)

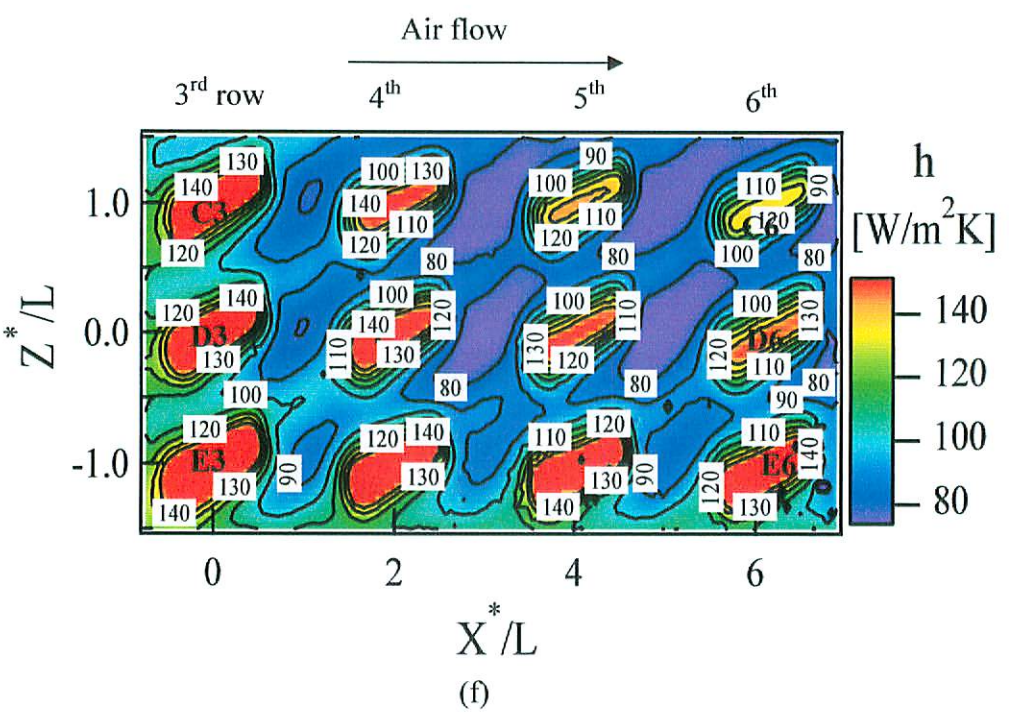

(f)

Fig. 6.1 Detailed heat transfer coefficient profile with iso heat transfer coefficient contour of the representative fin region with co-angular pattern for U= 10 m/s, H_f = 10 mm, PR = 2 and for duct height (H_d) of (a) 20 mm, (b) 25 mm, (c) 30 mm, (d) 35 mm, (e) 40 mm, (f) 45 mm and (g) 50 mm.

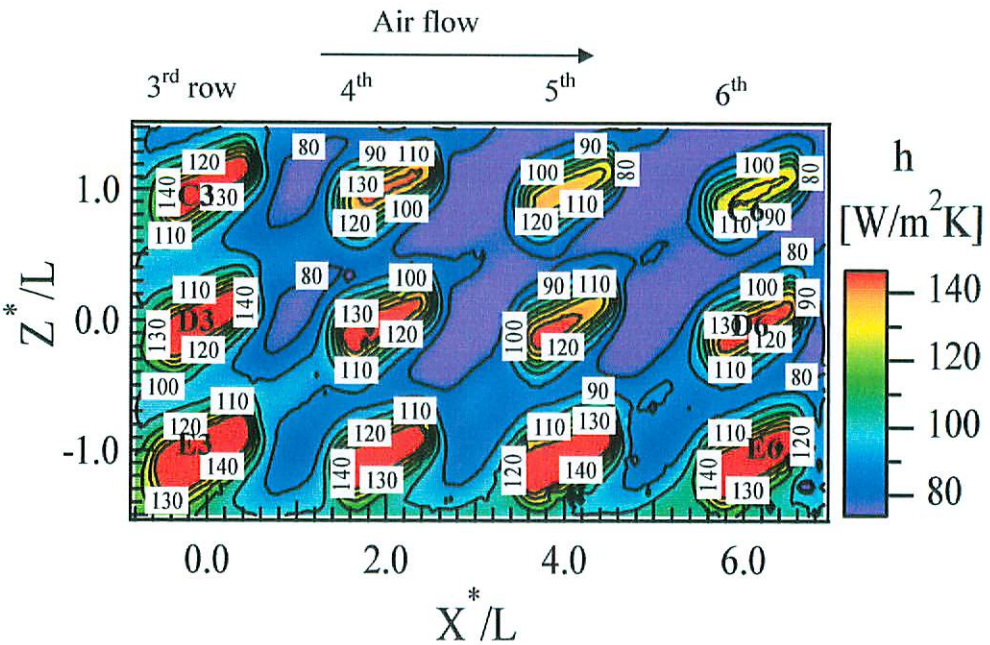

(g)

Fig. 6.1 Detailed heat transfer coefficient profile with iso heat transfer coefficient contour of the representative fin region with co-angular pattern for U= 10 m/s, H_f = 10 mm, PR = 2 and for duct height (H_d) of (a) 20 mm, (b) 25 mm, (c) 30 mm, (d) 35 mm, (e) 40 mm, (f) 45 mm and (g) 50 mm.

characteristics is changed with duct height. Now, we would like to observe the heat transfer coefficient profile with duct height in case of co-rotating pattern as shown in the following figure, Fig. 6.2. The shape of the heat transfer coefficient profile on the endwall for co-rotating pattern is completely different than that for the co-angular pattern. For all duct height shape of heat transfer coefficient profile is similar for co-rotating pattern. Iso heat transfer contour and heat transfer profile also shows that heat transfer increases with duct height and then decreases with increasing duct height and 25 mm duct experiences the highest heat transfer among the duct.

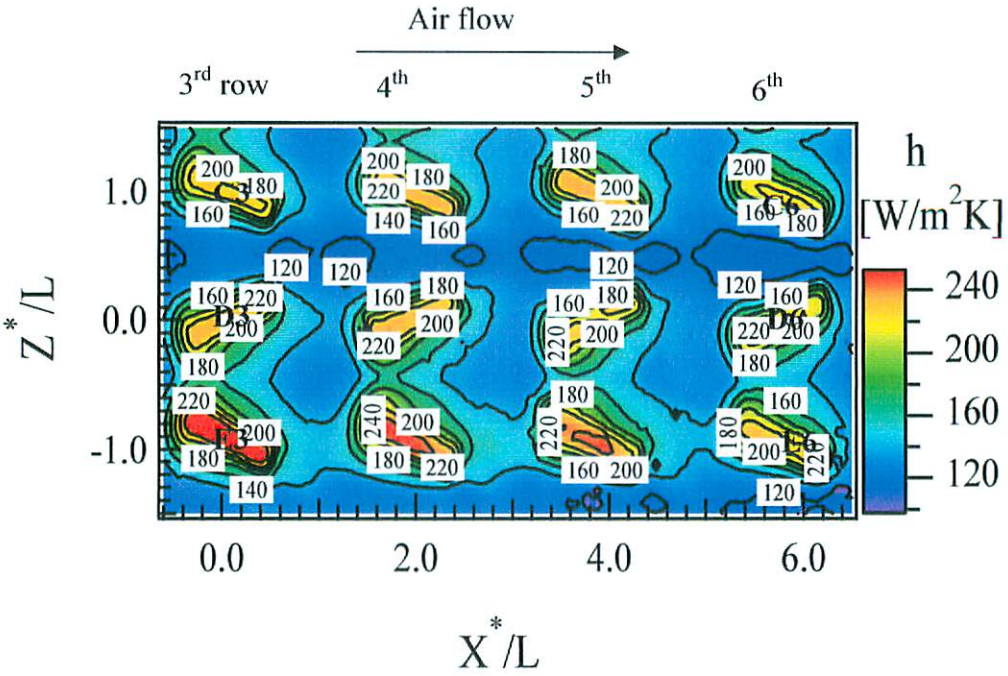

(a)

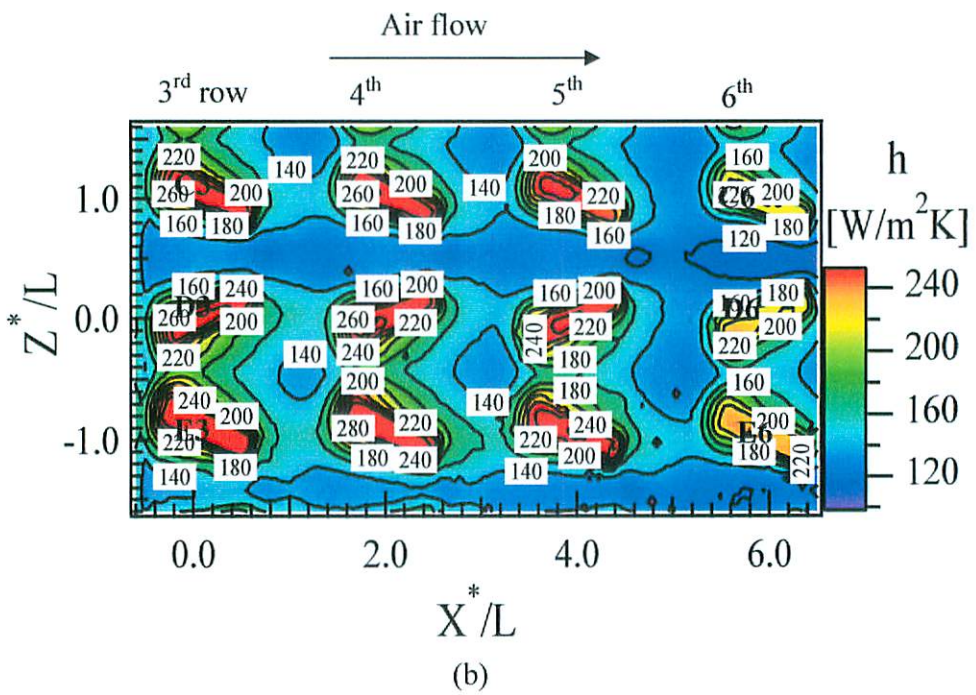

(b)

Fig. 6.2 Detailed heat transfer coefficient profile with iso heat transfer coefficient contour of the representative fin region with co-rotating pattern for U = 10 m/s, H_f = 10 mm, PR = 2 and for duct height (H_d) of (a) 20 mm, (b) 25 mm, (c) 30 mm, (d) 35 mm, (e) 40 mm, (f) 45 mm and (g) 50 mm.

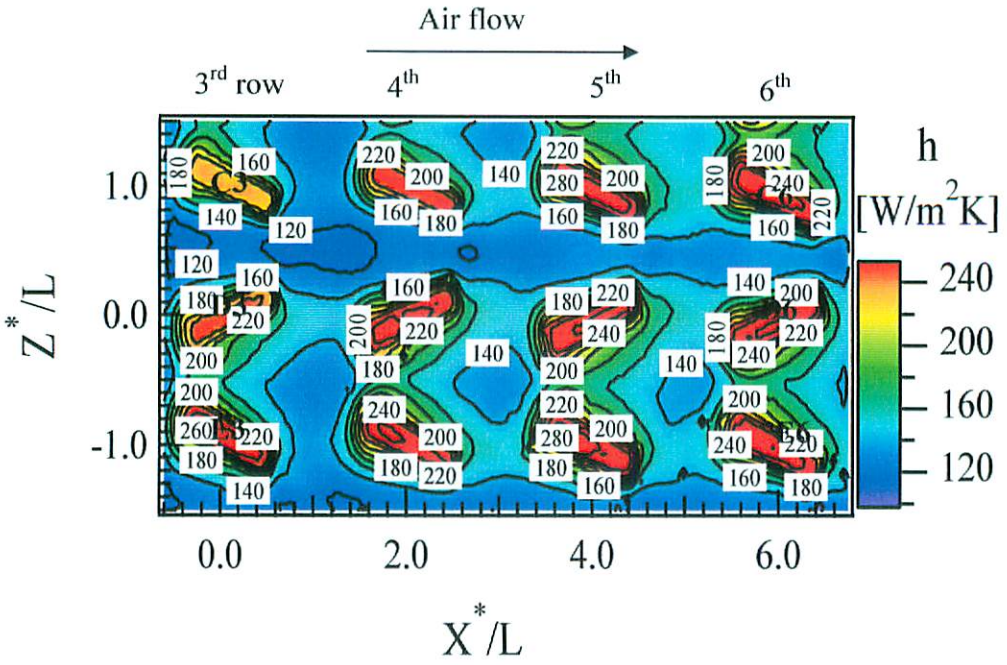

(c)

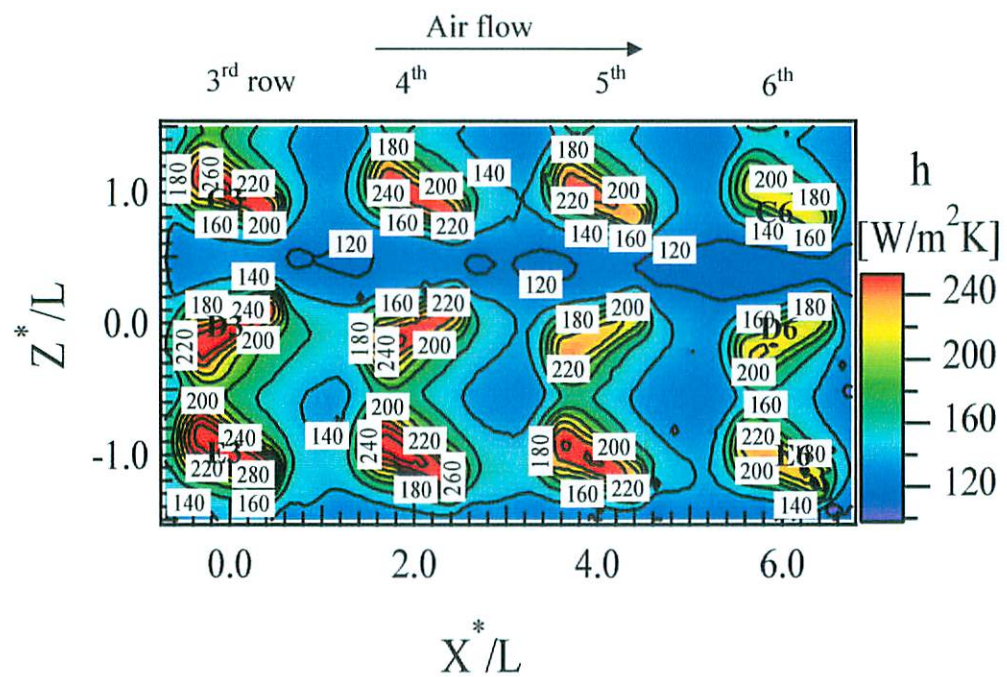

(d)

Fig. 6.2 Detailed heat transfer coefficient profile with iso heat transfer coefficient contour of the representative fin region with co-rotating pattern for U= 10 m/s, H_f = 10 mm, PR = 2 and for duct height (H_d) of (a) 20 mm, (b) 25 mm, (c) 30 mm, (d) 35 mm, (e) 40 mm, (f) 45 mm and (g) 50 mm.

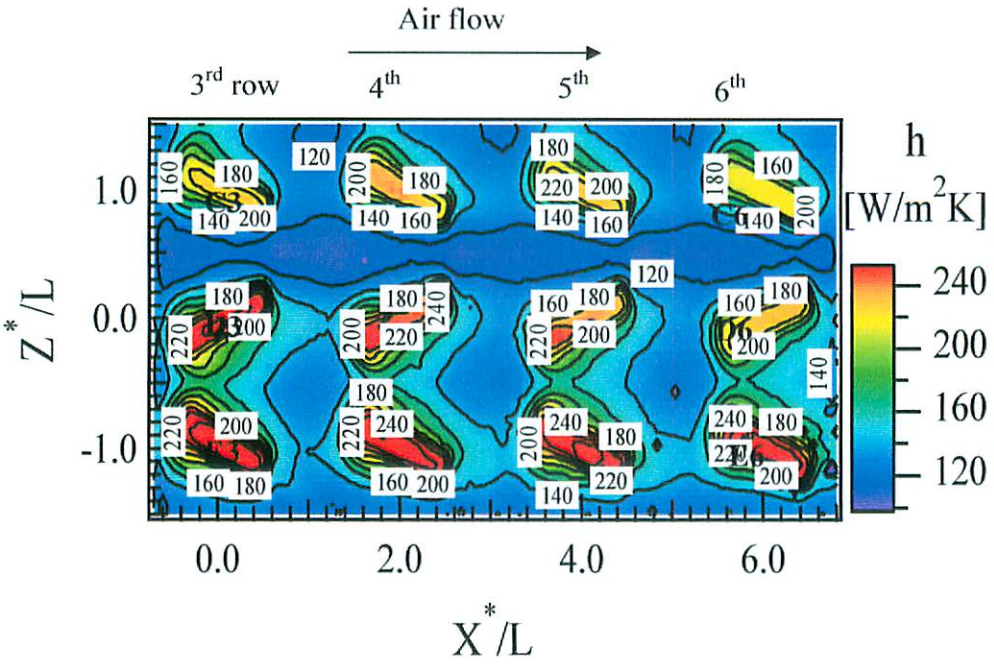

(e)

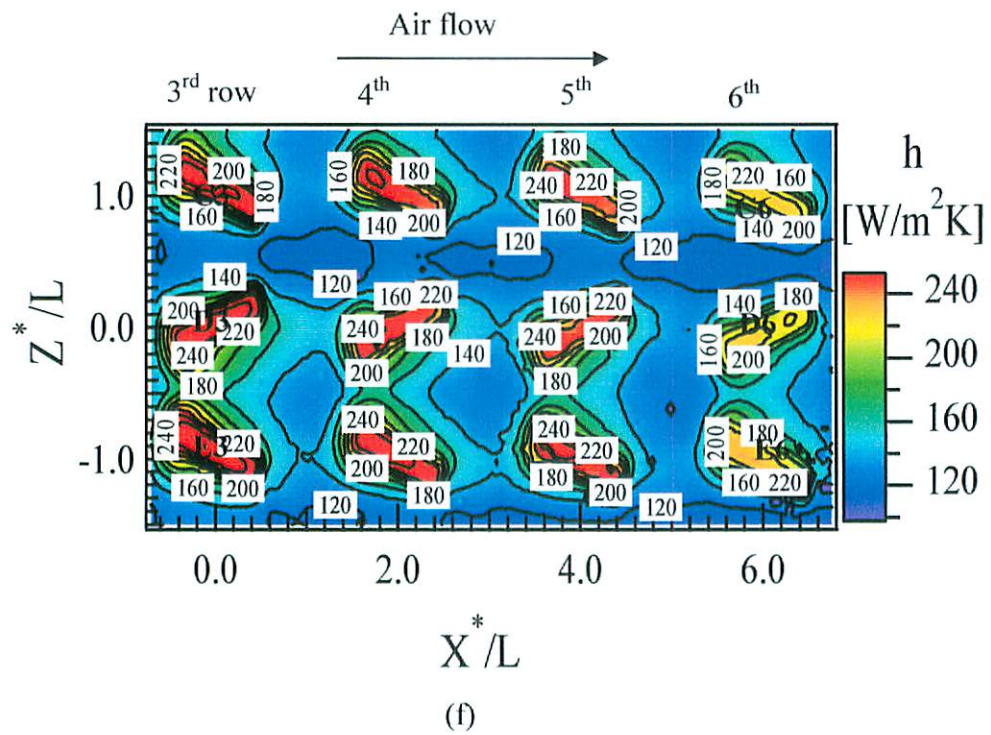

(f)

Fig. 6.2 Detailed heat transfer coefficient profile with iso heat transfer coefficient contour of the representative fin region with co-rotating pattern for U = 10 m/s, H_f = 10 mm, PR = 2 and for duct height (H_d) of (a) 20 mm, (b) 25 mm, (c) 30 mm, (d) 35 mm, (e) 40 mm, (f) 45 mm and (g) 50 mm.

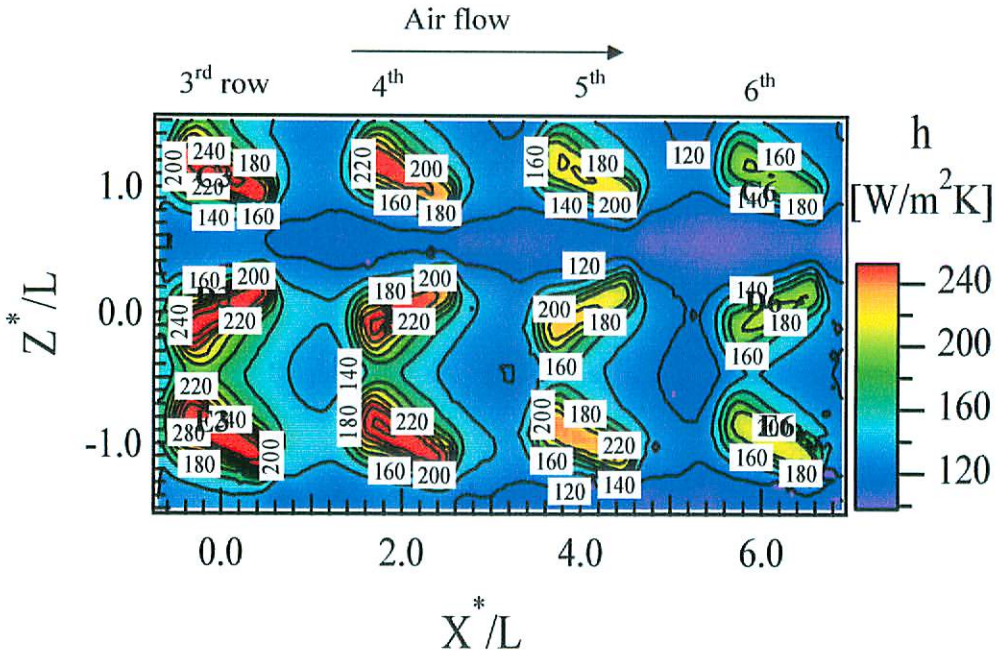

(g)

Fig. 6.2 Detailed heat transfer coefficient profile with iso heat transfer coefficient contour of the representative fin region with co-rotating pattern for U= 10 m/s, H_f = 10 mm, PR = 2 and for duct height (H_d) of (a) 20 mm, (b) 25 mm, (c) 30 mm, (d) 35 mm, (e) 40 mm, (f) 45 mm and (g) 50 mm.

In order to understand the heat transfer distributions more clearly, spanwise heat transfer distributions are drawn at some streamwise locations of the representative fin region. In Fig. 6.3 and Fig.6.4, spanwise heat transfer distributions are shown for all duct cases of co-angular pattern and co-rotating pattern respectively.

In case of co-angular pattern spanwise heat transfer distribution at the fin centers, i.e. X^*/L = 0, 2 and 4 is periodic. Higher peak values are located at the fin center positions and the lower peak values are positioned between the fins in spanwise direction, i.e. at Z^*/L = +0.5 and -0.5. At all duct height case higher peak values are sharper than the lower peak values and this sharpness decreases with increasing duct height and the heat transfer coefficient of the peak values gradually decreases in streamwise positions for all duct cases. Just behind the fins, i.e. at X^*/L = 0.5, 2.5 and 4.5 though periodical distribution appears, but it is remarkable that the lower

peak values are somewhat larger than for at fin center positions. This is expected because the vortex generated by plate fin touches the endwall (base plate) just after the fins which will be more clearly explained by streamwise flow visualizations. At the middle of the fin rows, i.e. $X^*/L = 1$ and 3, the shape of the profile is not distinctly periodical. Front of the fins heat transfer profile becomes periodical again. From Fig.6.3 it is shown that heat transfer coefficient profile at streamwise direction remains similar for all duct height with some differences in value.

Shape of the heat transfer coefficient profile of co-rotating pattern shows dissimilarity with co-angular one. Higher heat transfer coefficient distributions are achieved at a duct height of 25 mm as shown in Fig.6.3. Converging fin pairs causes higher heat transfer coefficient profile between fins in spanwise direction at $X^*/L = 0$, 2 and 4. Comparatively lower heat transfer distributions are appeared between diverging fin pairs at the same positions mentioned. The trends of distributions are almost similar at all duct height.

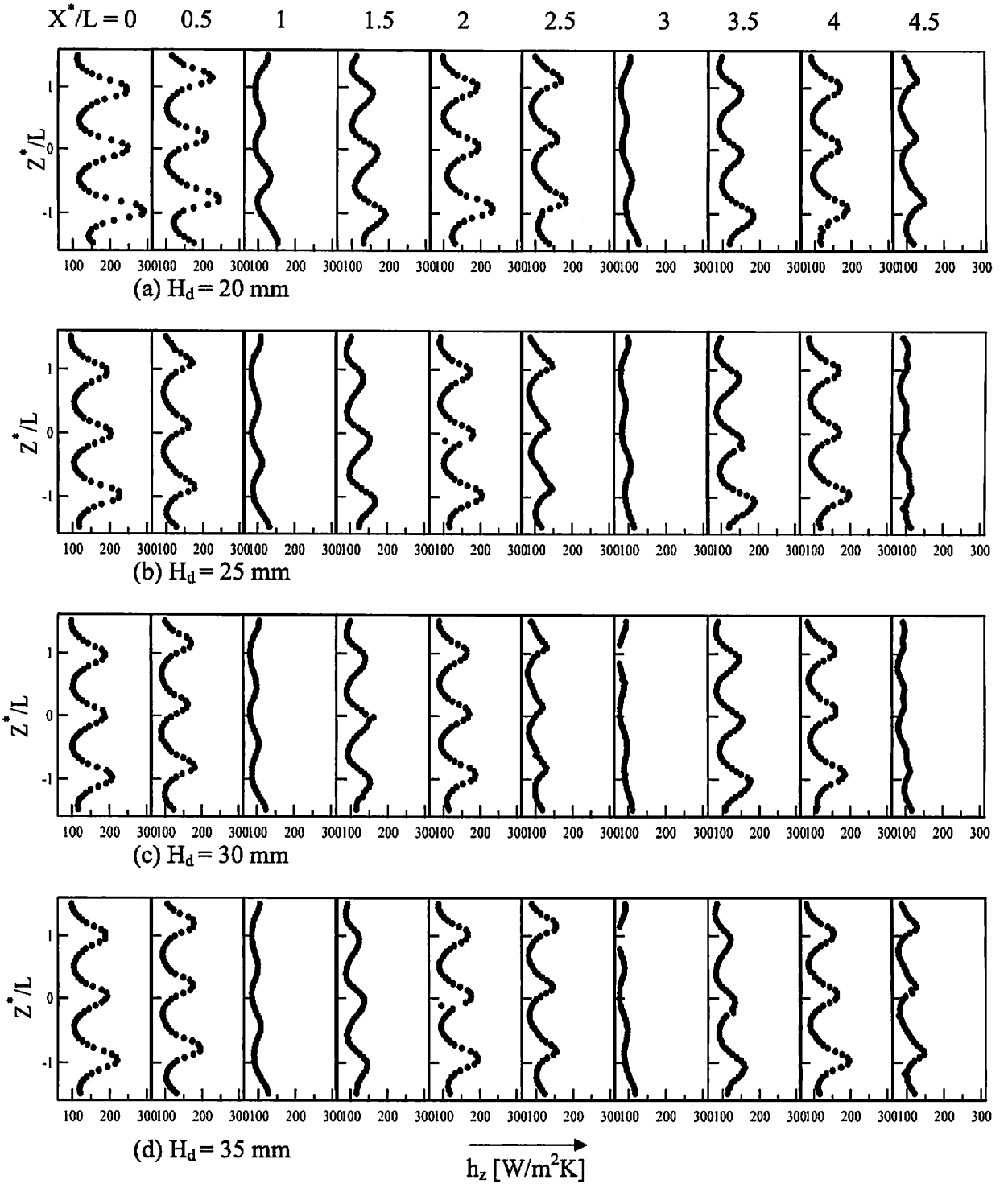

Fig. 6.3 Spanwise heat transfer coefficient distributions on the endwall with co-angular pattern for U=10m/s, H_f= 10 mm and of different duct height.

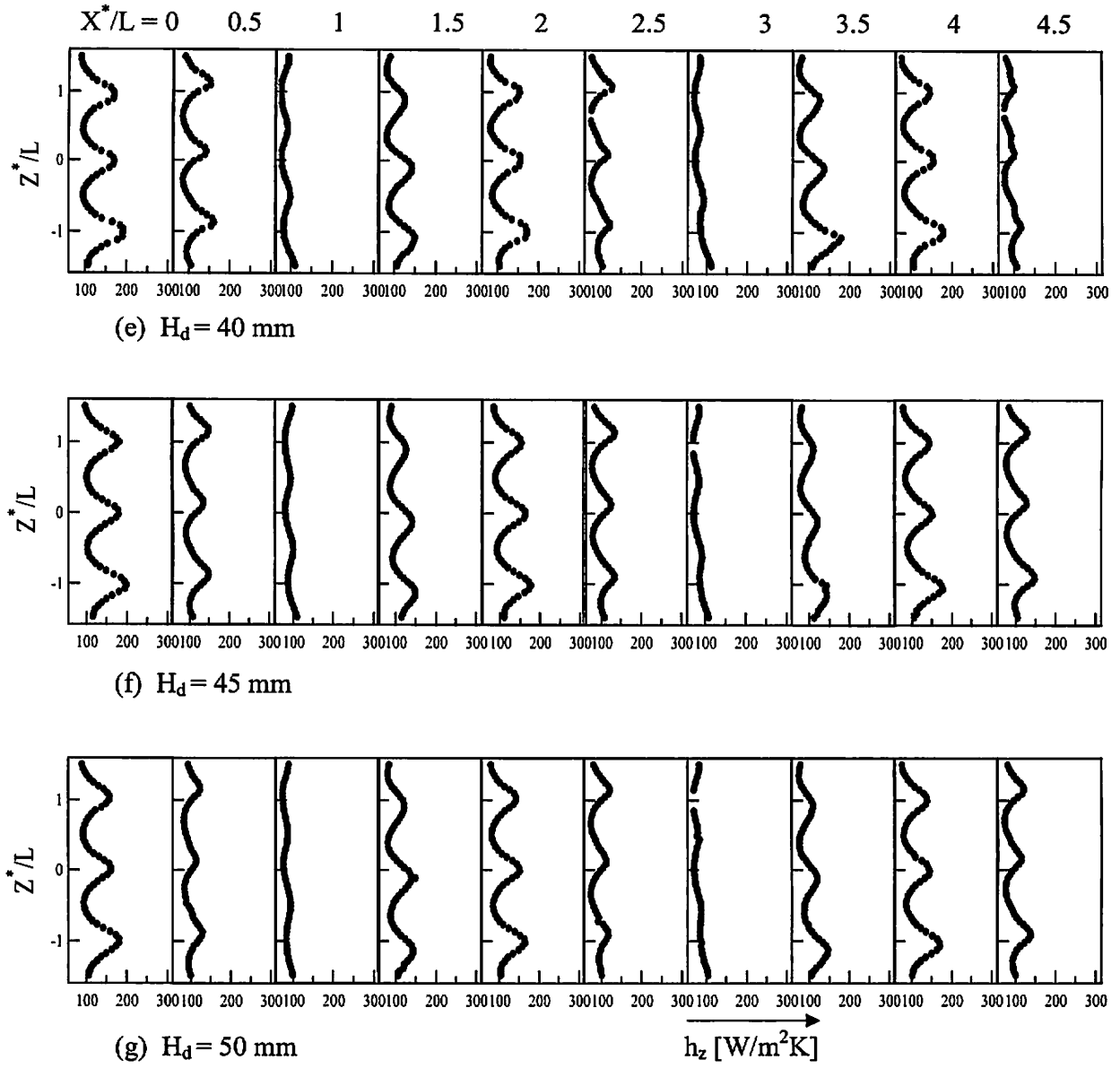

Fig. 6.3 Spanwise heat transfer coefficient distributions on the endwall with co-angular pattern for U=10m/s, H_f= 10 mm and of different duct height.

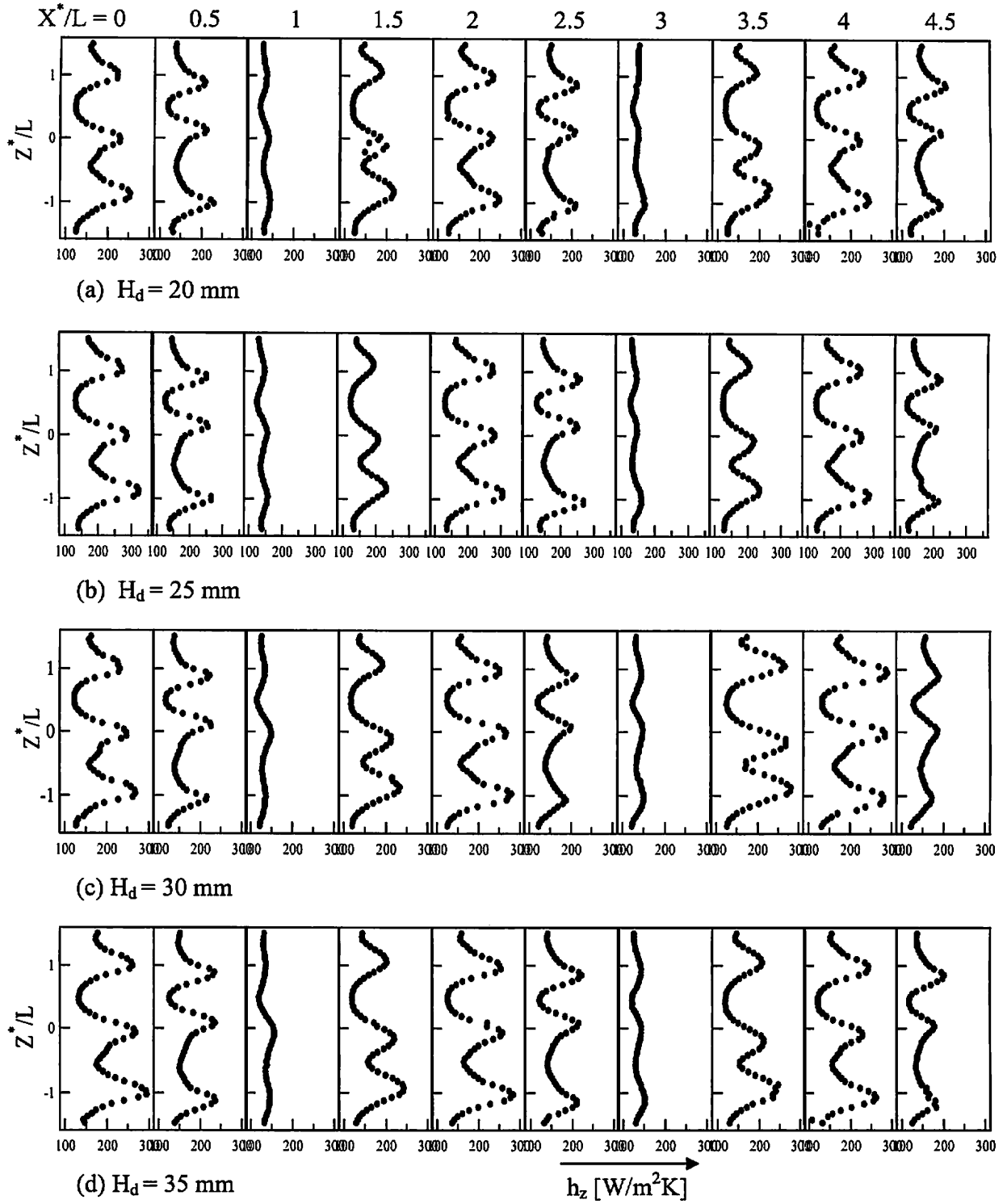

Fig. 6.4 Spanwise heat transfer coefficient distributions on the endwall with co-rotating pattern for U=10m/s, H_f= 10 mm and of different duct height.

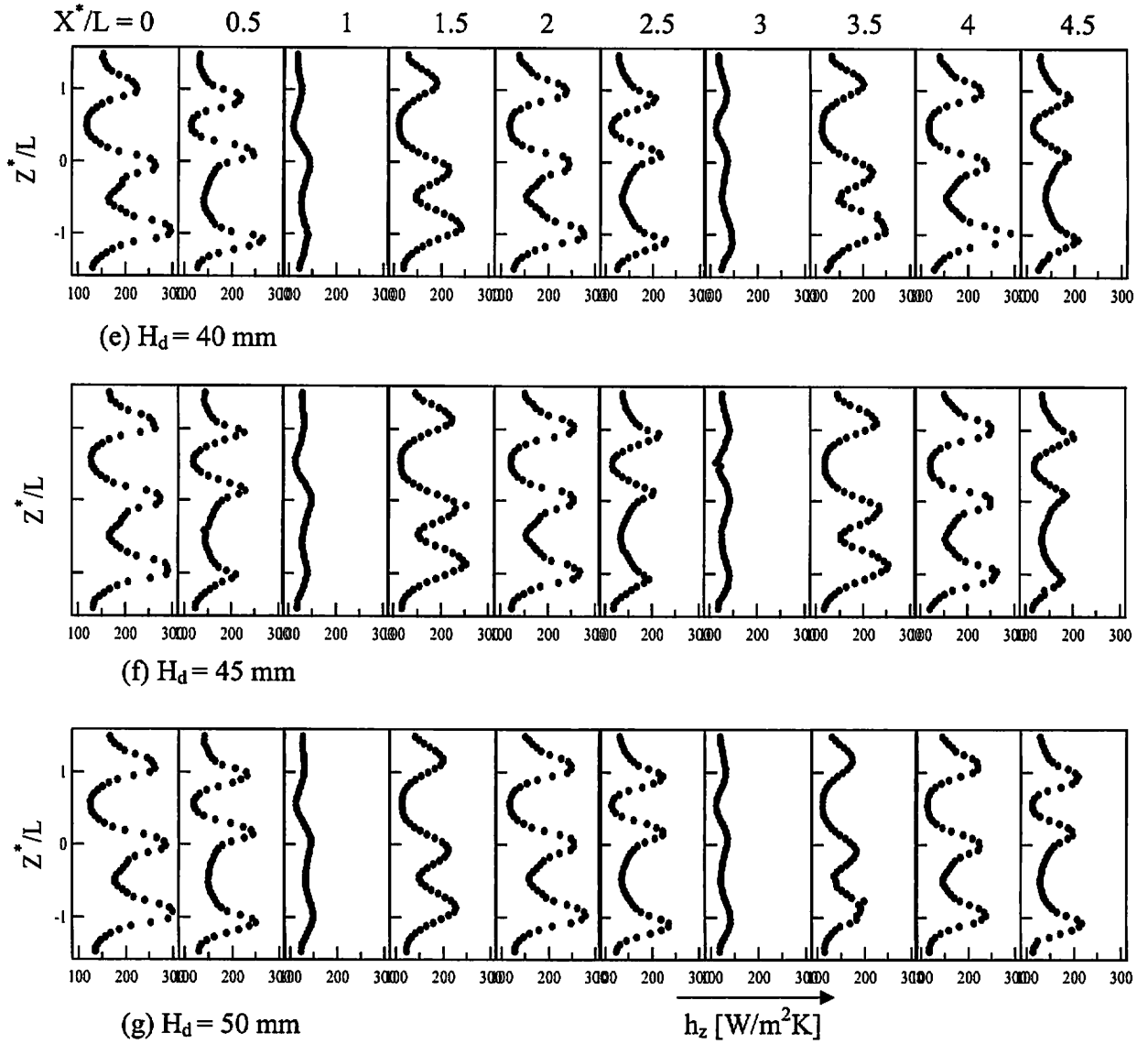

Fig. 6.4 Spanwise heat transfer coefficient distributions on the endwall with co-rotating pattern for U=10m/s, H_f= 10 mm and of different duct height.

6.3 Area averaged heat transfer coefficient and Nusselt numbers

We have estimated the area averaged heat transfer coefficient for the overall surfaces of the representative fin region for different duct height and fin pattern following the Eq.(4.3). And then we calculated average Nusselt number based on hydraulic diameter of the duct and average heat transfer coefficient. Area averaged heat transfer coefficients are then plotted against mainstream velocity. The area averaged heat transfer coefficients are further represented by the curve fitted lines and all the data fall smoothly on the curve fitted lines and can be well represented as the form of Eq. (4.4). In Fig.6.5 it is shown that area averaged heat transfer coefficient increases with mainstream velocity regardless of duct height and fin pattern. In case of co-angular pattern, are averaged heat transfer coefficient are decreasing with increasing the duct height and highest heat transfer values are obtained at 20 mm duct. But co-rotating pattern shows a different behavior. Heat transfer coefficients first increases with duct height and then decreases with increasing the duct height. Maximum heat transfer coefficients are achieved at 25 mm duct case.

Relationship between Nusselt number and Reynolds number for different duct height with co-angular pattern and co-rotating pattern is shown in Fig. 6.6and 6.7, respectively. As the Nusselt number is based on duct equivalent diameter, Nusselt values increases with duct height regardless of fin pattern and Reynolds number. In Fig.6.7 there shows a significant difference of Nusselt values between 20 mm and 25 mm duct height which is not distinct in case of co-angular pattern. Co-rotating pattern shows higher Nusselt numbers than that of co-angular pattern.

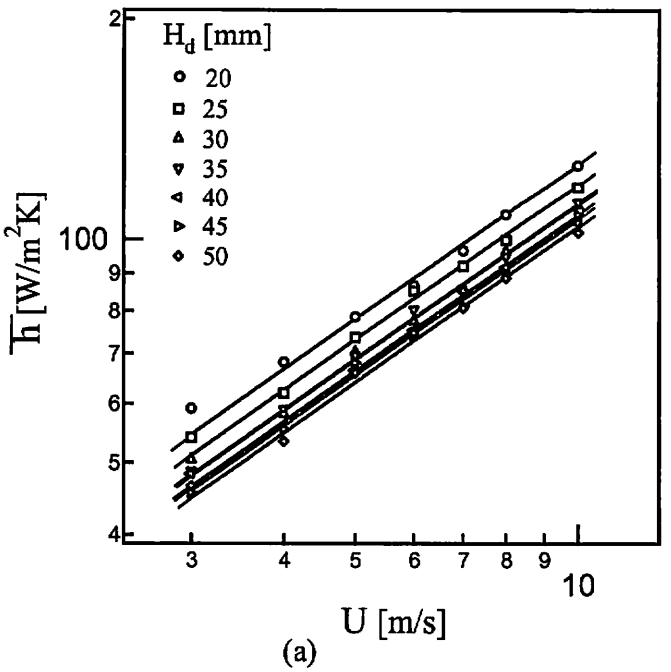

(a)

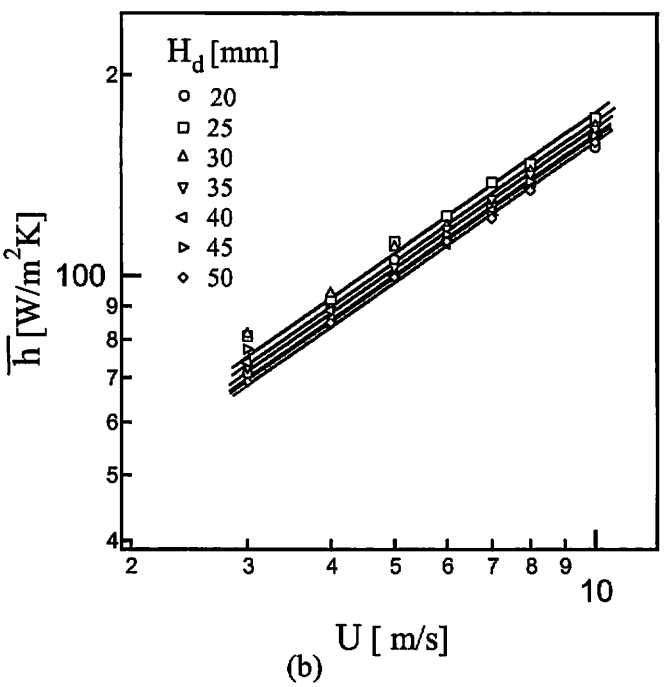

(b)

Fig. 6.5 Relation between area-averaged heat transfer coefficients, $\overline{h}$ and mainstream velocity, U at different duct height of (a) co-angular pattern and (b) co-rotating pattern

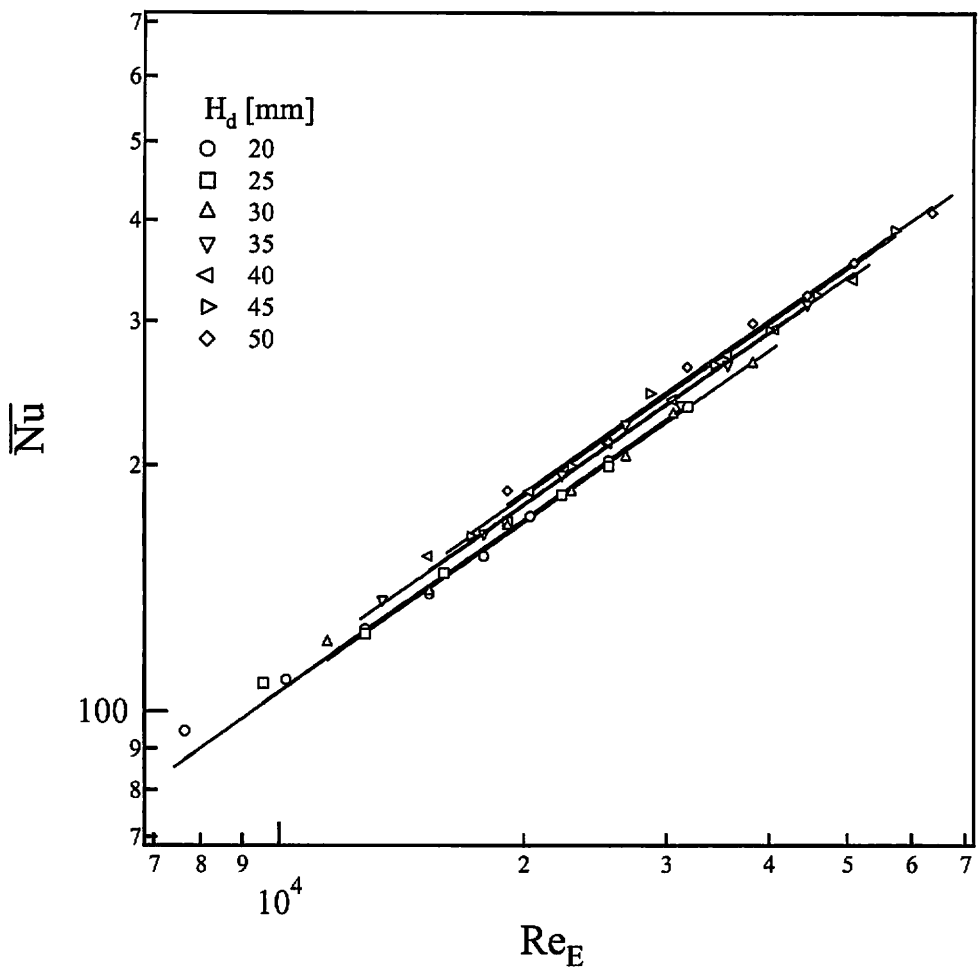

Fig. 6.6 Relationship between Nusselt number and Reynolds number with co-angular pattern at different duct height.

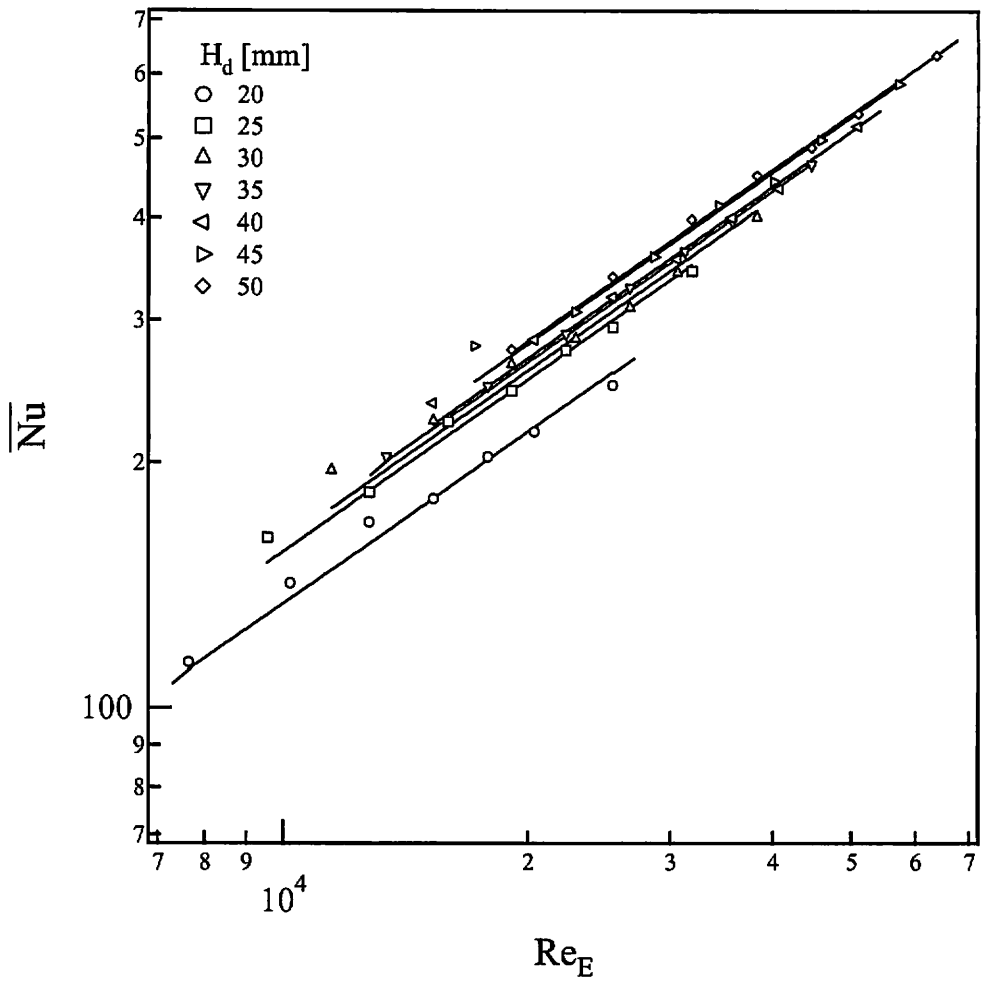

Fig. 6.7 Relationship between Nusselt number and Reynolds number with co-rotating pattern for different duct height.

6.4 Friction factor

To estimate a pressure drop as well as thermal performance with insertion of fins, the friction factor for different duct height and fin patterns were measured, and its result are presented in Fig. 6.8 and Fig. 6.9. Friction factor, f is obtained from Eq. (3.1). Friction factor decreases with increasing the duct fin height ratio (H_d/H_f) regardless of fin pattern and this is expected because the larger friction occurs for smaller duct fin height ratios. Co-rotating pattern experiences the larger friction factor than for co-angular pattern, because more turbulence and flow interactions are occurred in case of co-rotating pattern. When compare Fig.6.8 and 6.9, there shows a big difference of friction factor between duct fin height ratio (H_d/H_f) of 2 and 2.5 in case of co-angular pattern, but in co-rotating case the difference is comparatively smaller. In case of co-angular pattern friction factor slowly decreases with Reynolds number and this tendency continues for duct fin height ratio of 2 and 2.5. For the other duct fin height ratios, friction factor initially decreases with increasing the Reynolds number but finally slowly increases with Reynolds number.

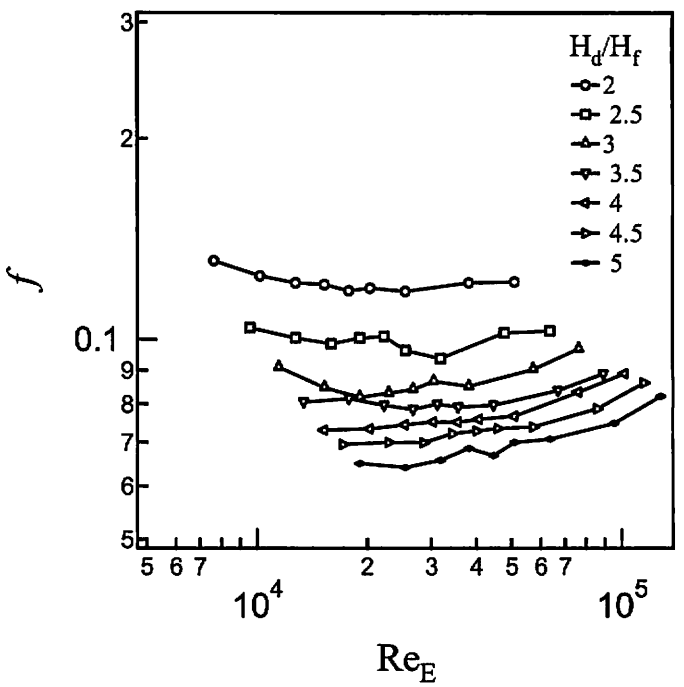

Fig. 6.8 Variation of friction factors with Reynolds numbers for co-angular pattern at different duct height.

The tendency of friction factor with Reynolds number is same as that of co-angular case up to duct fin height ratio of 2 and 2.5. For the larger duct fin height ratio, friction factor initially decreases with Reynolds number following almost constant value for the higher Reynolds number which is different behavior than for co-angular pattern.

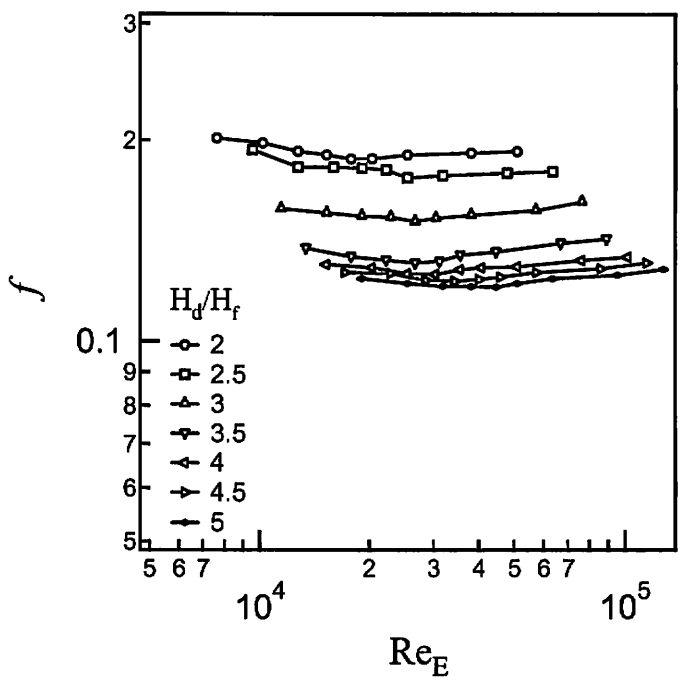

Fig. 6.9 Variation of friction factors with Reynolds numbers for co-rotating pattern at different duct height.

6.5 Vortex structure analysis

To obtain qualitative information on the flow pattern, vortex structures, size and reattachment positions, the flow was visualized by Nd: YAG laser sheet using smoke as a tracer supplied at entrance of the duct and a high speed camera (Phantom V7.1) shot the photographs. In this study vortex structures at several positions were observed for different duct height and pattern. But we have shown the vortex structures for the 20 mm duct only and compared the structures for co-angular and co-rotating pattern as an example. Fig. 6.10 shows the formation and variation of vortex structures at streamwise positions of X/L = 0, 0.5, 1, 1.5, 2, 3.5, 4.5 and 7 for the co-angular pattern. At X/L = 0 and 0.5 formation of longitudinal vortex is clearly observed at fin top surface which is then growing up at X/L = 1. Vortex pattern looks similar regardless of streamwise direction. At X/L = 2 vortex reattached to the endwall and the photograph shows that the vortex size is growing at further downstream. In the figure it is shown that the longitudinal vortex generated by the fin rotates and then downwash the surface strongly whereby enhance heat transfer. So it can be concluded that next fin setting at around X/L = 2 will be effective for heat transfer enhancement. In Fig 6.11 vortex structures at streamwise positions are shown for the co-rotating pattern. Vortex structures look different than that of co-angular pattern. Longitudinal behavior is also appeared for co-rotating case same as that of co-angular pattern. The photographs are arranged with same scale for both patterns. Closer observation indicates the different length of the origin of circulation for different pattern. In case of co-rotating pattern origin of the circulation vortex is closer around X/L = 1.5 and then slowly increases at further downstream wherein in co-angular pattern the closer point is around X/L = 2. In both cases the rotation of vortexes touched the endwall surfaces and enhances heat transfer. Vortex rotation in co-rotating case is larger compared to that of co-angular pattern.

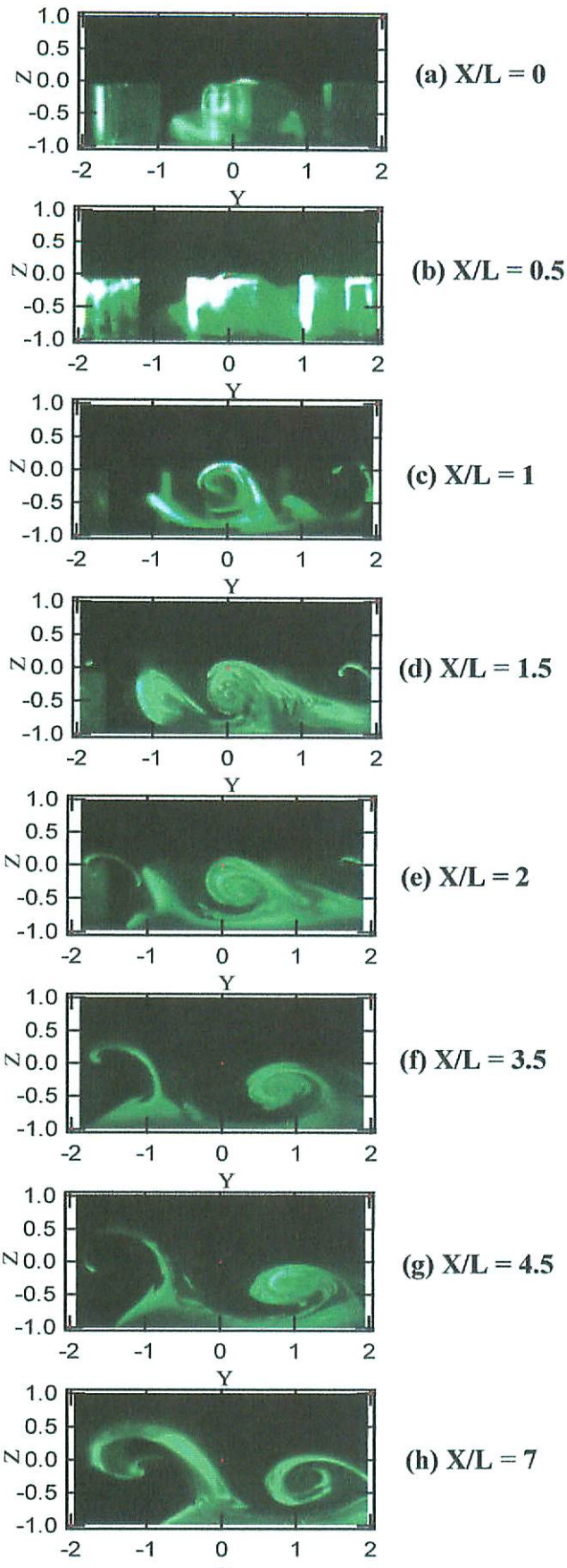

Fig. 6.10 Vortex structures at several streamwise positions with co-angular pattern at H_d = 20 mm

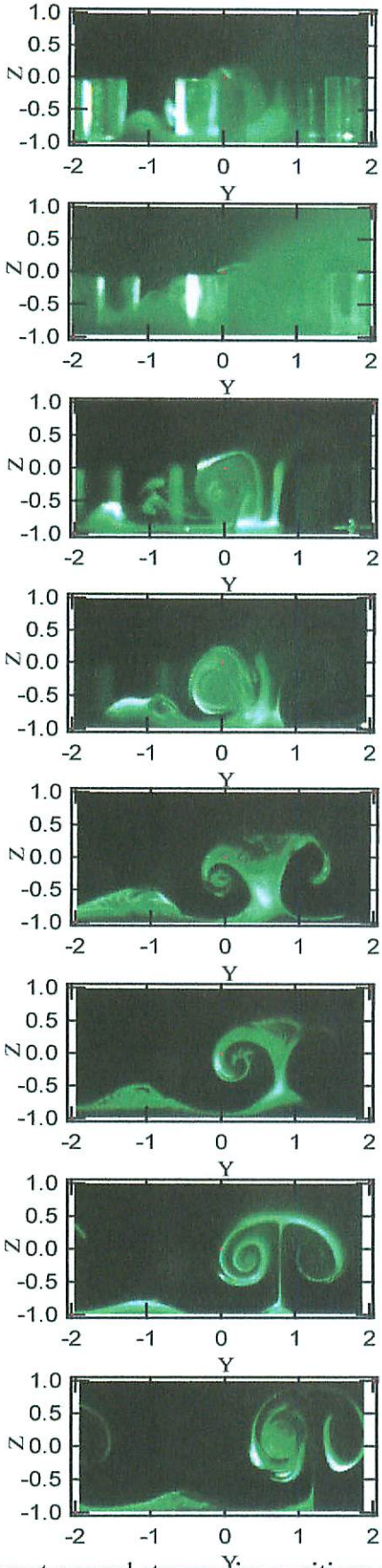

Fig. 6.11 Vortex structures at several streamwise positions with co-rotating pattern at H_d = 20 mm

6.6 Thermal performance ratio

As we already know the various technique [1974] to design the heat exchanger. In Fig.6.12 and Fig.6.13 the relationship between thermal performance ratio with Reynolds numbers is shown for co-angular pattern and co-rotating pattern respectively. Thermal performance decreases with Reynolds number regardless of duct fin height ratio and fin pattern. In general, it is seen that η possesses the higher value for all duct height case at the lower regime of $f^{1/3}Re$, regardless of fin patterns and its value reaches nearly 3 and 4 for co-angular and co-rotating pattern respectively. Thermal performance ratio of co-rotating pattern is comparatively higher than for co-angular pattern. The differences of thermal performance ratios for different duct heights are almost even in co-angular case. But for co-rotating pattern there shows a big difference for smaller duct fin height ratio, i.e for H_d/H_f= 2, 3 and 3.5. Except these ratios a very little difference in thermal performance ratio is appeared. Next we investigate the effect of duct height on thermal performance and get the most optimum duct height by comparison with a reference duct height. The following relation is obtained under the constant pumping power condition when a reference duct is expressed with sub index "*ref*"

$$f^{\frac{1}{3}}\,\mathrm{Re}(H_{dref}/H_d) = f^{\frac{1}{3}}\,\mathrm{Re}_{ref} \text{ ----------(5.6)}$$

where H_{dref} denotes a reference duct height, then the heat transfer augmentation or thermal performance ratio $\acute{\eta}$ is expressed as follows:

$$\acute{\eta} = \bar{h}/\bar{h}_{ref} \text{ ----------(5.7)}$$

We select H_d= 20 mm as a reference duct height, the data for relative performance ratio $\acute{\eta}$ based on Eq.(5.7) is shown as a function $f^{1/3}\,\mathrm{Re}_{ref}$ in Fig.6.14 and 6.15.

So from the the relative performance graph it is clear that for co-angular pattern 20 mm duct is the most optimum for the highest thermal performance. The other effect of duct height on the relative performance is found that thermal performance decreases with increasing the duct height

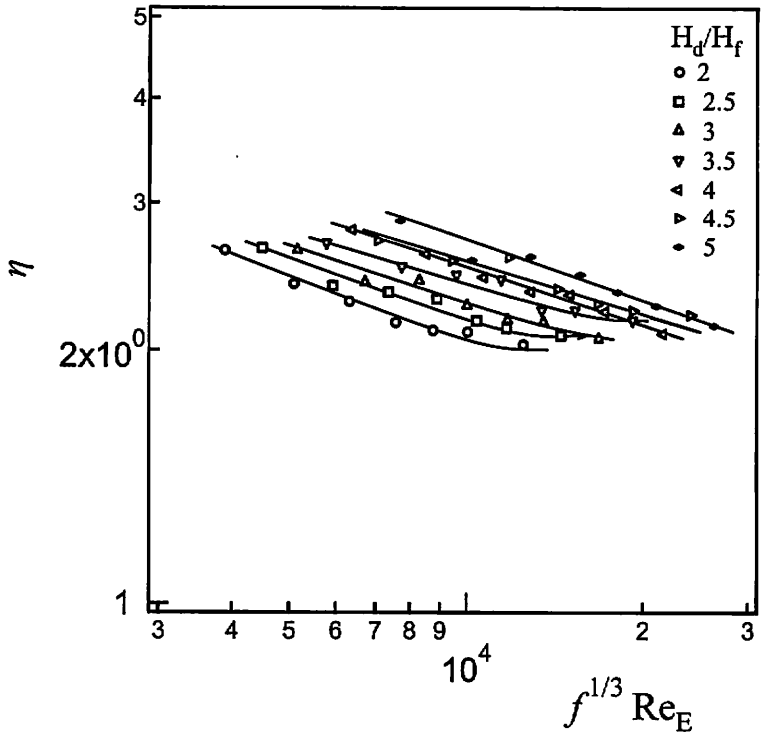

Fig. 6.12 Thermal performance ratio with Reynolds number for co-angular pattern at different duct fin height ratio.

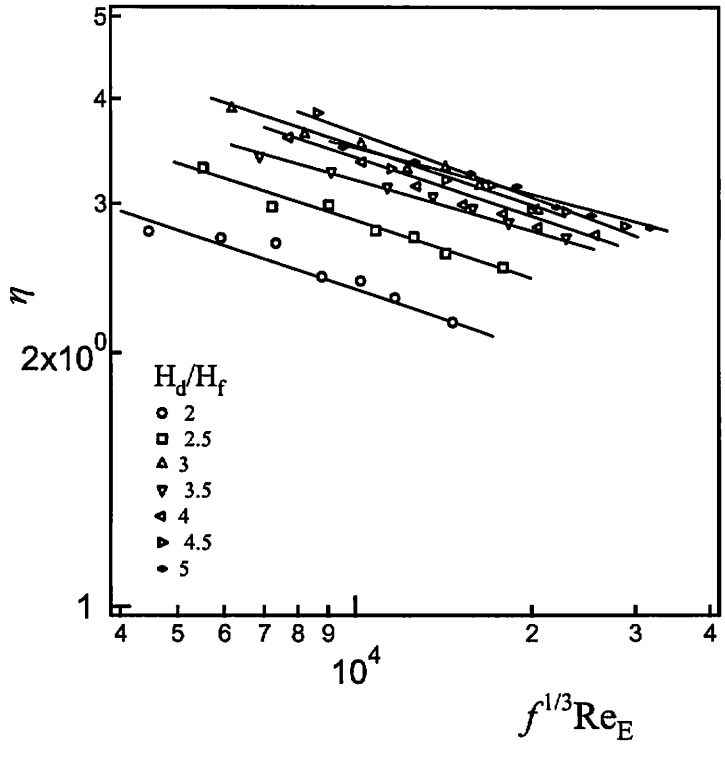

Fig. 6.13 Thermal performance ratio with Reynolds number for co-rotating pattern at different duct fin height ratio.

in case of co-angular pattern. For the co-rotating pattern, the effect of duct height on the relative performance is different than that of co-angular pattern. Here, initially the relative performance increases with increasing the duct height and 25 mm duct height shows the highest relative performance. After then relative performance decreases with increasing the duct height.

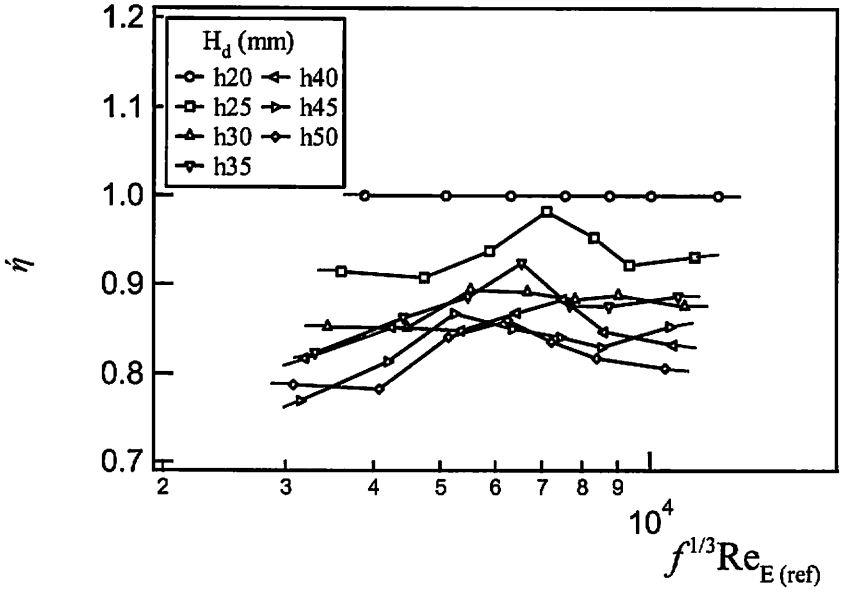

Fig.6.14 Effect of H_d on the relative performance evaluation for the co-angular pattern.

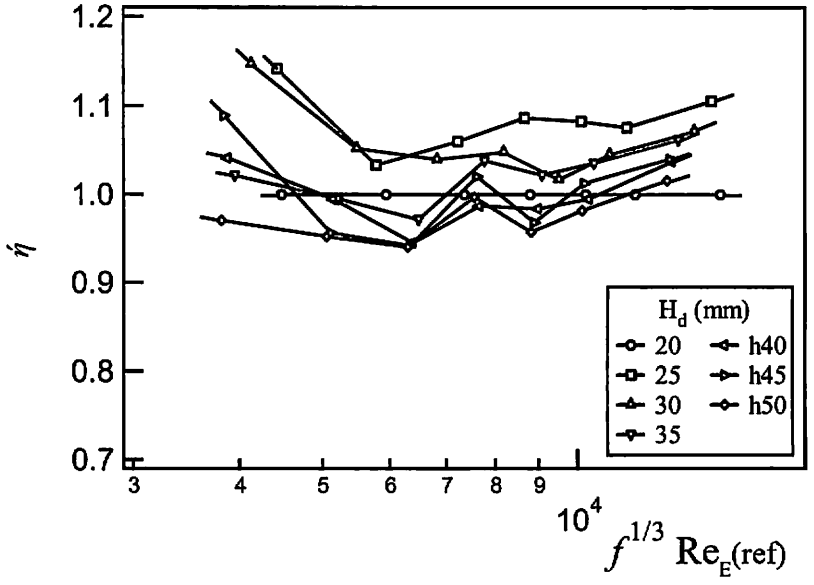

Fig.6.15 Effect of H_d on the relative performance evaluation for the co-rotating pattern.

6.7 Summary

In this chapter we mainly discussed the effects of duct height on heat transfer and flow characteristics. After thorough investigation we can summaries as follows:

(1) Iso heat transfer coefficient profile along with detailed heat transfer distributions gives a complete idea how the duct height influences the heat transfer from the endwall for the different pattern.

(2) The area averaged heat transfer coefficient on the overall surfaces (including fin base) increases with velocity regardless of duct height and fin pattern. In case of co-angular pattern, are averaged heat transfer coefficient are decreasing with increasing the duct height and the highest heat transfer values are obtained at 20 mm duct. But co-rotating pattern shows a different behavior. Heat transfer coefficients first increases with duct height and then decreases with increasing the duct height. Maximum heat transfer coefficients are achieved at 25 mm duct case.

(3) The relative performance graph shows 20 mm and 25 mm duct is the most optimum for the highest thermal performance for co-angular and co-rotating pattern respectively. The other effect of duct height on the relative performance is found that thermal performance decreases with increasing the duct height for the co-angular pattern where as for co-rotating case, initially the relative performance increases with increasing the duct but finally decreases with increasing the duct height.

(4) Friction factor slowly decreases with Reynolds number regardless of duct fin height ratio for co-rotating pattern where in co-angular case this behavior exists only for duct fin height ratio of 2 and 2.5.

(5) The most important information about vortex structures at several streamwise positions is obtained which shows the reasons of heat transfer enhancement. Vortex structures for co-angular and co-rotating pattern are found different and the reattachment positions are obtained. Vortex rotation in co-rotating case is larger compared to that of co-angular pattern which is responsible for heat transfer enhancement.

7

Conclusions

In this thesis we have discussed heat transfer and fluid flow characteristics of finned surfaces. Inclined short rectangular fins of four different patterns and arrangements are investigated in duct flows and the relative magnitudes of the extended surface and the vortex generator effect are determined. Flow behavior and different types of vortexes as well as vortex structures which causes the heat transfer enhancement are observed by different flow visualization technique. After thorough investigation we have the following conclusions:

(1) The effect of inclination angle on heat transfer showed that the heat transfer coefficient for 20° inclination angle is comparatively larger among the three, 0°, 20° and 25° which agrees with the data obtained by Bilen et al. [2002].

(2) The effect of fin height on area averaged Nusselt number ($\overline{Nu}_{overall}$) for smallest *PR* and co-rotating pattern shows that 10 mm fin has the maximum value and the difference of Nusselt number between 10 mm and 15 mm fin is very little. The same effect was also observed in case of co-angular pattern [2007].

(3) At a narrow duct, the area averaged Nusselt numbers on overall surface area ($\overline{Nu}_{overall}$) increases with increasing the Reynolds number regardless of fin patterns and pitch ratio (*PR*). Among the four patterns, co-rotating pattern has the highest Nusselt number and the co-angular pattern has the least Nusselt number. The effect of pitch ratio on heat transfer shows that $PR = 2$ have the highest Nusselt value and the value is decreased with increasing *PR* for all fin patterns.

(4). When the thermal performance is considered, Higher thermal performance occurred

in the following order, co-rotating, co-counter rotating, zigzag and co-angular pattern. Co-rotating pattern with PR = 2 and H_f = 10 mm is the most recommended configuration since it produces the highest overall heat transfer enhancement with slightly higher pressure penalty due to the pronounced vortex effect on both the endwall and fin surfaces. Heat transfer augmentation with co-rotating pattern is more than three times the fin-less duct.

(5) Detailed heat transfer coefficient distributions from the infrared image of representative region gives a complete idea of higher heat transfer area and lower heat transfer area. Spanwise heat transfer coefficient profile and streamwise heat transfer coefficient profile implies the heat transfer characteristics of different fin patterns.

(6) The friction factors for all fin patterns are larger compared to the skin friction on the smooth surface for a fully developed turbulent flow. Among the four patterns largest friction factor was developed for the co-rotating pattern owing to the strong flow interactions and combined vortex attack on the endwall and fin surface whereas the least friction developed for co-angular pattern. Friction factor value is slowly decreased with increasing Reynolds number and pitch ratio, PR.

(7) Dye flow in water channel, Oil titanium oxide film flow and smoke flow visualizations confirmed the longitudinal vortex, horse shoe vortex, corner vortex and other vortexes generated by all fin patterns which cause the heat transfer enhancement.

(8) Smoke flow pattern around the fins and oil titanium oxide film flow pattern on the endwall shows a good agreement with each other. Horseshoe vortex is shown apparently dominant in case of co-angular fin pattern whereas in case of zigzag fin pattern wavy flow behavior was observed. In case of co-rotating fin pattern more tortuous flow is observed as the longitudinal vortexes generated by diverging fin pairs combinedly attack the endwall and fin surfaces. This flow was somewhat disturbed by the following converging fin pairs in case of co-counter rotating fin pattern.

(9) The effects of duct height on heat transfer for co-angular and co-rotating patterns were also observed. In that case, it was found that the area averaged heat transfer coefficient on the overall surfaces increases with velocity regardless of duct height and fin pattern. In case of co-angular pattern, area averaged heat transfer coefficient decreases with increasing the duct height and the highest heat transfer values are obtained at 20 mm duct whereas co-rotating achieved the maximum heat transfer coefficients at 25 mm duct.

(10) The relative performance graph also shows 20 mm and 25 mm duct is the most optimum for the highest thermal performance for co-angular and co-rotating pattern respectively. The other effect of duct height on the relative performance is found that thermal performance decreases with increasing the duct height for the co-angular pattern where as for co-rotating case, initially the relative performance increases with increasing the duct but finally decreases with increasing the duct height

(11) Friction factor slowly decreases with Reynolds number regardless of duct fin height ratio for co-rotating pattern where in for co-angular case this behavior exists only for duct fin height ratio of 2 and 2.5.

(12) Vortex structures for co-rotating pattern and co-angular pattern at several streamwise positions were traced out by smoke flow which gives new information about the reattachment positions of the longitudinal vortexes. Comparatively large scale vortex rotation is observed in co-rotating case which is obviously responsible for heat transfer enhancement.

References

Bergles, A.E. et al. (1974), Performance evaluation criteria for enhanced heat transfer surfaces,Proc. 5th Int'l Heat Trans Conf., Tokyo, Vol 2, pp. 239.

Bilen, K., Yapici,S. (2002) Heat transfer from a surface fitted with rectangular blocks at different orientation angle, Heat and Mass Transfer, Vol. 38, pp. 649-655.

El-Saed, S.A., Mohamed, S.M., Abdel-Latif, A.M.and Abouda, A.E. (2002) Investigation of turbulent heat transfer and fluid flow in longitudinal rectangular fin-arrays of different geometries and shrouded fin array, Experimental Thermal and Fluid Science, Vol. 26, pp. 879-900.

Edwards, F.J. and Alker, C.J.R.(1974), The improvement of forced convection surface heat transfer using surface protrusions in the form of (a) cubes and (b) vortex generators, Proceedings of the 5th International Heat Transfer Conference, Tokyo, vol.2, pp 244-248.

Fiebig, M., Kallweit, P. and Mitra, N.K.(1986), Wing type vortex generators for heat transfer enhancement, Heat Transfer, C.L Tien et al. ed., Hemisphere, Washington, vol. 6, pp. 2909-2913

Fiebig, M., Kallweit, P., Mitra, N. and Tiggelbeck, S.,(1991), Heat transfer enhancement and drag by longitudinal vortex generators in channel flow, Experimental Thermal and Fluid Science, vol. 4, no.1, pp 103-114.

Fiebig, M., Valenica, A. and Mitra, N.K.,(1993), Wing type vortex generators for fin-and-tube heat exchangers, Experimental Thermal and Fluid Science, vol. 7, pp 287-295.

Fiebig, M., Valenica, A. and Mitra, N.K.,(1994),local heat transfer and flow losses in fin-and-tube vortex generators: a comparison of round and flat tubes, Experimental Thermal and Fluid Science, vol. 8, pp 35-45.

Herman, C. (1994) Experimental visualization of temperature fields and measurement of heat transfer enhancement in electronic system models, In: S Kakac; H Yuncu; K Hijikata (eds) Cooling of Electronic systems, NATO ASI Series 258, Kluwer Academic, Dedrecht,pp. 313-337

Herman, C. and Kang, E., (2001) Experimental visualization of temperature fields and study of heat transfer enhancement in oscillatory flow in a grooved channel, Journal of Heat Mass Transfer, Vol. 37, pp. 87-89.

Igarashi, T. (1983), Local heat transfer from a square prism to an air stream, International Journal of Heat and Mass Transfer, Vol. 29, No. (5), pp. 777-784.

Islam, M.D., Oyakawa, K. and Yaga, M. (2006) Fluid flow and infrared image analyses on endwall fitted with short rectangular plate fin, Journal of Thermal Science, Vol.15,No.2, pp. 145-151.

Islam, M.D., Oyakawa, K., Yaga, M. and Senaha, I. (2007) Study on heat transfer and fluid flow characteristics with short rectangular plate fin of different pattern, Experimental Thermal and Fluid Science, Vol.31, pp. 367-379.

Kadle, D.S., Sparrow, E.M. (1986) Numerical and experimental study of turbulent heat transfer and fluid flow in longitudinal fin array, ASME J. of Heat Transfer, Vol.108, pp. 16-23.

Molki, M., Faghri, M. and Ozbay, O. (1995) A correlation for heat transfer and wake effect in the entrance region of an inline array of rectangular blocks simulating electronic components, ASME Journal of Heat Transfer, Vol.117, pp. 40-46.

Matsumoto, R., Kikkawa, S. and Senda, M., (1997). Effect of pin fin arrangement on end wall heat transfer, JSME International Journal Series B, 40(1), pp 142-151

Oyakawa, K., Furukawa, Y., Taira, T and Senaha, I. (1993). Effect of vortex generators on heat transfer enhancement in a duct, Proceeding of the Experimental Heat Transfer, Fluid Mechanics and Thermodynamics, Honolulu, Hawaii, pp. 633-640.

Sparrow, E.M. and Saboya, F.E.M, (1976) Transfer characteristics of two-row plate fin and tube heat exchanger configurations, International Journal of Heat and Mass Transfer, Vol.19, pp 41-49.

Sparrow, E.M., Niethammer, J.E. and Chaboki, A.(1982). Heat transfer and pressure drop characteristics of arrays of rectangular modules encountered in electronic equipment, Int. J. of Heat Mass Transfer, Vol.25, pp. 961-973.

Sparrow, E.M., Vemuri, S.B. and Kadle, D.S. (1983) Enhanced and local heat transfer, pressure drop, and flow visualization for arrays of block-like electronic components, Int. J. of Heat Mass Transfer, Vol.26, pp. 689-699.

Turk, A.Y. and Junkhan, G.H (1986) Heat transfer enhancement downstream of vortex generators on a flat plate, Heat Transfer, C.I. Tien et al. ed., Hemisphere Washington, Vol. 6,pp. 2903-2908.

Torii, K. and Yanagihara, JI.(1997) A review on heat transfer enhancement by longitudinal vortices, Journal HTSJ, Vol.36, No.142, pp. 73-86

Van Fossen, G.J. (1982) Heat transfer coefficients for staggered arrays of short pin fns, Journal Engineering Power, 104, pp 268-274

Webb, R.L. and Eckert, E.R.G. (1972) Application of rough surfaces to heat transfer exchanger design, Int. J. of Heat and Mass Transfer, Vol.15, pp. 1647-1657.

Acknowledgements

At the concluding stage of my long time study and research here at Okinawa, Japan, I would like to thank them all who helped and supported me in various ways for successful completion of my Doctoral course. I am grateful to my Lord, Lord of the universe who made everything ease for me and my family during this period. At first I express deep gratitude to my honorable supervisor Dr. Kenyu Oyakawa, professor of mechanical systems engineering, University of the Ryukyus, under whose supervision and proper guidance this work is carried out. I am extremely grateful for his constant support, encouragement and the most valuable time he spent during this research. I sincerely thank my professor for arranging the research fund during my critical time when I was really in need of financial help.

I am very grateful to Dr. Minoru Yaga, professor of mechanical systems engineering for his support, encouragement, valuable suggestions and help to solve the problem at any difficulty, especially for reviewing my research papers. I sincerely thank Dr. Izuru Senaha, Associate professor of mechanical systems engineering for his support in arranging experimental facilities at the laboratory. I express sincere respect to Professor T. Nosoko, who taught me advanced heat transfer and thermodynamics in my Doctoral course work. I will not forget Mr. Oshiro, technician of machine shop/factory, who constantly co-operate me in making experimental apparatus at the factory and helped me friendly at practical problems whenever required.
Thanks to all of the graduate and undergraduate students of my laboratory for their hearty co-operation. I am ever grateful to HNF, HEIWA NAKAJIMA FOUNDATION for awarding me scholarships in this research work.

At this moment I remember the most wonderful time and events enjoyed with my family here in Okinawa. How can we forget the most beautiful Island, where my son, Islam Mohammed Shamiul was born while my daughter, Islam Fariha grown up slowly with the fresh air. Finally I would like to thank my beloved wife, Shathi for her long term patience and support during this work. I really enjoyed life and study in Okinawa with having such a good companion. I am waiting to see my mother and family member in Bangladesh.